Interpreting Echo Statistics of Three Distinct Clutter Classes Measured With a Midfrequency Active Sonar: Accounting for Number of Scatterers, Scattering Statistics, and Beampattern Effects

Timothy K. Stanton, Dezhang Chu, James M. Gelb*, Member, IEEE*, George L. Tipple*, Student Member, IEEE*, and Kyungmin Baik

Abstract—A recently developed published approach to predict echo statistics is applied to clutter data that were collected with a midfrequency sonar and published in a separate independent study. This method explicitly accounts for the (finite) number of unresolved scatterers, the statistics associated with the arbitrary scattering properties of the individual scatterers [but assumed to have identical echo probability density functions (pdfs) in this application], and beampattern effects which significantly affect the echo statistics due to each scatterer being randomly located in the sonar beam. The data had been categorized according to whether they were associated with bottom structures, diffuse compact clutter, and compact nonstationary (moving) clutter. In this paper, the recently developed method is incorporated in a two-component mixed pdf (mixed with a Rayleigh distribution to account for the diffuse background) to model the statistics of the three classes of clutter. This is the first such application of the model which had principally been validated only numerically. The degree to which the data are non-Rayleigh (heavy tailed) is reasonably predicted by the model and the number of scatterers per resolution cell is inferred for each type of clutter.

Index Terms—Beampattern, clutter, non-Rayleigh reverberation, reverberation statistics.

I. INTRODUCTION

A key challenge in using an active acoustic system to detect a scatterer or "target" of interest is to distinguish the target echo from the interfering echoes or "clutter" caused by surrounding scatterers that are not of interest. Generally, the more the statistics of the clutter echoes deviate from being Rayleigh distributed (i.e., become "heavy tailed"), the more they will tend

to interfere in the detection process. Thus, it is important to have accurate models of the echo statistics of clutter in order to quantify the probability of false alarm of the target.

There is a variety of general statistical descriptions of clutter fields, regardless of whether they involve sonar or radar systems, or volumetric or surficial clutter fields. These include the K-distribution [1]–[3] and generalized Pareto distribution (GPD) [4], [5]. In a recent study by Gelb *et al.*, both of these distributions were used to characterize the statistics of clutter data collected with a long-range midfrequency active sonar [5]. "Midfrequency," in this application, is defined as any frequency in the range 1–10 kHz. The clutter data were divided into three distinct classes of echoes as being due to bottom-like (BL), compact stationary (CS), and compact nonstationary (moving) (CNS) features, and parameters from each probability density function (pdf) were determined. The data were demonstrated to be strongly non-Rayleigh (heavy tailed), and there was generally good qualitative agreement between the shape of the data and theoretical distributions.

A limiting factor in the analysis in [5] was the fact that physical parameters of the scattering and sonar were not explicitly described in the theoretical pdfs with the exception, to some extent, of the K-distribution. The shape parameter of the K-distribution has been shown to be related to the number of scatterers for the case of an exponential distribution of scatterer echoes after beampattern effects and a negative binomial distribution of number of scatterers, although not explicitly including beampattern effects [2]. Because of these limitations and, in spite of the success of matching the shapes of theoretical pdfs to the clutter data, it would be a challenge to make predictions of clutter echo statistics based on this analysis. For example, since the GPD has no physical interpretation, changes in the echo statistics due to any change in the scattering geometry such as range, sonar beamwidth, number of unresolved clutter features, and change in distribution of sizes of individual clutter features could not be predicted. With the K-distribution, although some of the above changes could be predicted, the predictions would be based on the assumption that the distribution of echoes after beampattern effects from individual clutter features remained exponentially distributed. If they are not exponentially distributed, then the shape parameter may be interpreted as an effective number of scatterers.
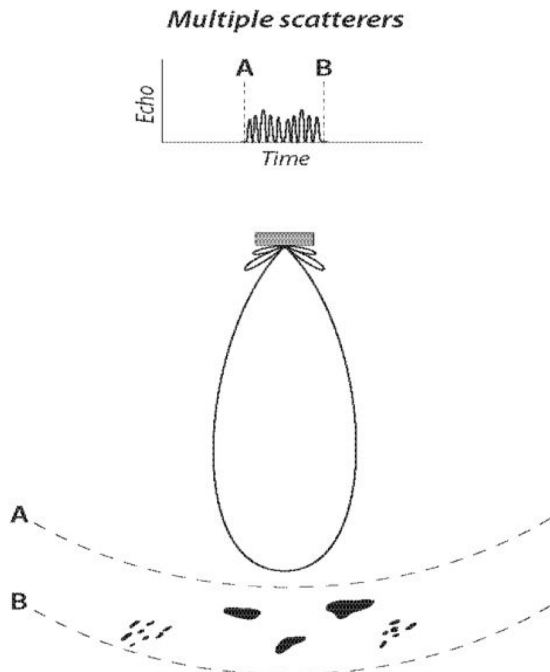
Fig. 1. Scattering geometry for N scatterers or small patches of scatterers randomly distributed in a sonar beam. In this formulation, a small unresolved patch of scatterers is treated as a single scatterer.

In a separate and independent study, Chu and Stanton have recently addressed the above limitations by deriving the echo statistics from first principles in terms of statistics associated with random scattering properties and sonar parameters [6]. Specifically, an echo measured by the sonar is modeled as being due to the coherent summation of echoes from N unresolved individual clutter features, each with their own echo pdf before beampattern effects, and each randomly located in the sonar beam (Fig. 1). This is for the geometry in which the only echoes are from the clutter features and there are no unwanted reflections from neighboring boundaries. That is, these are the so-called "direct path" echoes. With each scatterer having its own (arbitrary) echo pdf before beampattern effects, this is in sharp contrast to the above K-distribution in which the echoes after beampattern effects are limited to having an exponential pdf. Furthermore, the random weighting due to the random location of each feature in the beam is explicitly accounted for, which significantly affects the echo statistics. The approach is exact and general, as the quantities N, individual echo pdfs, and the sonar beampattern are arbitrary and rigorously accounted for. Predictions of the echo pdf, as seen through the sonar receiver (that is, including beampattern effects) and due to the summation of the individual echoes, were made through both analytical and numerical calculations in that paper (although there were no applications to experimental data). The echo pdfs were demonstrated to be strongly non-Rayleigh, owing to a combination of both the finite number of scatterers and the beampattern effects. Specifically, the tails of the pdfs were elevated over the Rayleigh pdf, especially as N became small.

The beampattern plays a major role in causing the non-Rayleigh effects. In addition to reducing the effective number of scatterers causing the echo, the nonuniform weighting is equally important. For example, the sum of a small

number of independent signals, each Rayleigh distributed and of equal mean, will also be Rayleigh distributed, no matter how small the number is. However, for a small number of scatterers randomly distributed in the sonar beam, each with a Rayleigh distributed echo (before beampattern effects) and with an equal mean, once summed, is strongly non-Rayleigh [6]. This is true even if the locations of the scatterers are limited to being within the mainlobe of the beam because of the significant variations in weighting from the center of the beam down to near the null.

As described above, clutter data were presented in [5] which exhibited strongly non-Rayleigh properties, but lacked physical interpretation. Published at the same time was the new model which could interpret the degree to which the data are non-Rayleigh in terms of the number of scatterers, the statistics associated with their random scattering properties, and sonar parameters [6]. However, the model had only been validated numerically at the time and had not been applied to experimental data. In this current paper, the clutter data presented in [5] are revisited through the use of the recently developed general approach from [6]. The work serves to provide a physical interpretation of the clutter data using the new model as well as serves as a basis of experimental validation of the model. Since environmental data were not collected in the experiment, the validation is limited to qualitative analysis such as comparing the shape of the predicted pdfs to those of the experimental pdfs. Because of the lack of environmental data, a simplifying assumption is made in which the clutter features have identical echo pdfs. With this assumption and through rigorous accounting of beampattern effects, the number of scatterers per resolution cell is estimated from the echo statistics data for each type of clutter feature. Part of the modeling involved accounting for the diffuse background scattering through the use of a mixture pdf such as in the work of Abraham *et al.* [7], [8].

II. THEORY

The recently developed method in [6] for determining the statistics of the echo magnitude $\tilde{e}$ due to N arbitrary scatterers, each randomly located in a beam, is based on

$$\tilde{e} = \left| \sum_{i=1}^{N} \tilde{e}_i e^{j\Delta_i} \right| \tag{1a}$$

where

$$\tilde{e}_i = |f_i| b(\theta_i, \phi_i). \tag{1b}$$

For narrowband ($\sim$single frequency) signals such as in this paper, the magnitude $\tilde{e}$ is simply the amplitude of the acoustic sine wave. It is calculated by taking the square root of the sum of the squares of the real and imaginary components of $\tilde{e}$ [i.e., the absolute value as shown in (1a)]. The term $\tilde{e}_i$ is the magnitude of the echo from the ith scatterer as seen through the eyes of a monostatic sonar (i.e., with beampattern effects), Δ_i is the phase associated with each scatterer (including the contribution associated with the range from the sonar, scattering by the object, and beamformer), f_i is the scattering amplitude of the ith scatterer [where the target strength (TS) of the scatterer is given by $\text{TS}_i = 20 \log |f_i|$], b is the value of the beampattern whose values lie in the range 0–1, θ_i and ϕ_i are the angular locations

of the ith scatterer in the beam, and $j = \sqrt{-1}$. The beampattern value b is the product of the transmit beampattern (b_t) and receive beampattern (b_r). The maximum value of the (composite) beampattern ($b = 1$) corresponds to the center of the mainlobe while $b = 0$ corresponds to the value of the nulls.

The signal is assumed to be narrowband in that all N echoes are completely overlapping when sampled. The processing (time) window is designed so that all scatterers described in (1) are assumed to be far enough away from the sonar so that the spreading losses associated with all scatterers are approximately the same (i.e., they all reside in a relatively thin hemispherical shell whose thickness corresponds to the sample time window). For simplicity, terms that all scatterers have in common such as source level, spreading loss, and receive sensitivity are suppressed, as is the time dependence. These common terms are eliminated through normalization of the signals, as discussed in Section III. The shell is thick enough relative to the acoustic wavelength so that the range-specific phase of each randomly located scatterer is assumed to be randomly and uniformly distributed $[0 \ 2\pi]$. The total phase Δ_i of the echo from each scatterer is the sum of the range-specific phase, the phase due to its scattering properties, and the phase associated with the beamformer. However, since the range-specific phase is already randomly and uniformly distributed $[0 \ 2\pi]$, then Δ_i is also randomly and uniformly distributed $[0 \ 2\pi]$.

Note that N is the total number of scatterers in the half-space within the hemispherical shell at range r. This is inherent to rigorously modeling the echoes, as the sonar system "sees" all scatterers in the half-space. For a typical narrow mainlobe, N is much larger than the number of scatterers subtended by the mainlobe in that shell. Thus, most scatterers in this formulation are, on average, in the sidelobes. This number will be scaled below when analyzing data to calculate the number of scatterers within the mainlobe.

Although the beampattern is a deterministic quantity, the location (θ_i, ϕ_i) of the scatterer in the beam is random. A function of a random variable is also a random variable and the beampattern function $b(\theta_i, \phi_i)$ is treated in this analysis as a random variable, with an associated beampattern pdf p_b, as illustrated (Fig. 2) [9]. This beampattern pdf was derived by Ehrenberg in his formulation to calculate echo statistics associated with a single scatterer randomly located in a beam [10]. Application and reviews of the Ehrenberg echo statistics work are given in [6] and [11]–[17].

The beampattern pdf is shown to be generally monotonically decreasing with increasing echo amplitude (Fig. 2). The fine structure is associated with the sidelobes. The section involving a constant slope (power law) for the values of normalized echo amplitude of just below unity and higher are associated with the portion within the mainlobe higher than the highest sidelobes.

The transducer used in the predictions in Fig. 2 is modeled to match the rectangular one used in the experiment: $ka = 8$ and $kb = 31.85$ where a and b are the half-width and half-length of the transducer, respectively, and k is the acoustic wave number ($= 2\pi/\lambda$, where λ is the acoustic wavelength). This corresponds to a one-way beamwidth of $5° \times 20°$. The same transducer is used to transmit and receive. The beampattern pdf in Fig. 2 is calculated using [10, eq. (B1)] and involves the entire range of
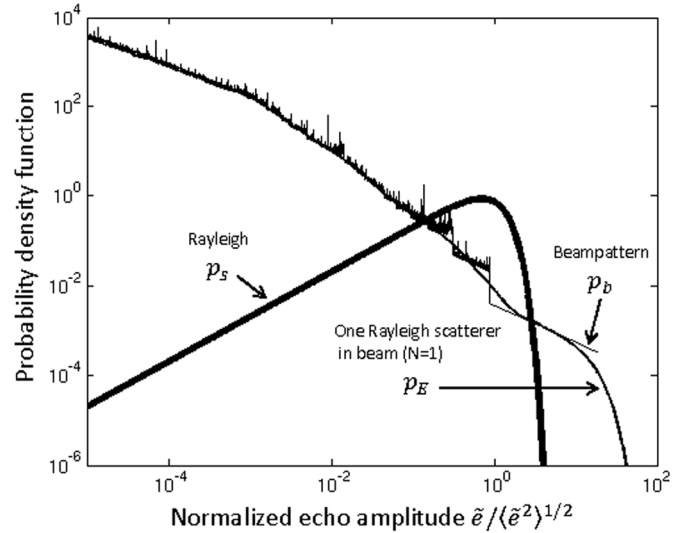

Fig. 2. Terms from (2) associated with echo statistics for one scatterer randomly located in a sonar beam. The pdf p_s of the magnitude of the scattering amplitude of the scatterer (i.e., echo before beampattern effects) for the case in which the general term p_s is set equal to the Rayleigh pdf in this example, beampattern pdf p_b, and the resultant echo pdf p_E as measured with the sonar (i.e., echo including beampattern effects) are shown. A rectangular aperture was used to form the $5° \times 20°$ beam.

values of beampattern, including sidelobes, and is plotted on a normalized scale. Since Ehrenberg's (B1) involves an echo intensity pdf, it was adapted to the case of echo amplitudes in this paper through a simple substitution of g^2 for g^4 ("g" is Ehrenberg's notation for this paper's $\sqrt{b}$).

As discussed above, the beampattern pdf for this rectangular aperture is generally monotonically decreasing and with fine structure associated with the sidelobes. At the upper range of echo amplitudes (right-hand side of curve), the section of pdf follows a power law and is associated with contributions from the mainlobe. These characteristics are qualitatively similar to those of previous studies involving circular transducers. Specifically, in [6] and [10], the monotonically decreasing power law section associated with the mainlobe of the beam was illustrated explicitly. In [10], beampattern pdfs were calculated for transducers of several different beamwidths. It was shown that, while the slope of the pdf remained constant with respect to beamwidth, the y-intercept varied (i.e., height of the "tail"). Also note that, although only the mainlobe portion of the beampattern pdf in [6] was shown (and on an unnormalized scale), the calculations of echo statistics in that paper involved the entire beam (that is, including all sidelobes). In a more recent study, the beampattern pdf for the entire beam (including sidelobes) for circular transducers is calculated for a range of beamwidths [14, Ch. 3]. That study also demonstrated how the pdfs remained qualitatively similar as the beamwidth changed, with the amount of fine structure associated with the sidelobes increasing with decreasing beamwidth.

The magnitude of the scatterer amplitude $|f_i|$ of each scatterer is also a random variable, independent of b, and with an associated pdf p_s. The statistics of the echo magnitude $\tilde{e}_i$ from the ith scatterer, when treated in isolation (i.e., not including echoes from all other scatterers), is calculated with the standard method associated with the product of two independent random

variables, i.e., $|f_i| b(\theta_i, \phi_i)$ in (1b) [9]. Ehrenberg applied that general formulation to the sonar problem to predict echo statistics associated with a single (ith) scatterer

$$p_E(\tilde{e}_i) = \int_{\tilde{e}_i}^{\infty} \frac{1}{x} p_s(x) p_b\left(\frac{\tilde{e}_i}{x}\right) dx, \qquad 0 \le b \le 1 \qquad (2)$$

where the standard formula was rewritten slightly by Ehrenberg in terms of a convolution integral through a simple substitution [10]. The term b is implicit in (2) through the relation $b = \tilde{e}_i / x$. In this formulation, the echo pdf was explicitly connected to sonar parameters (beampattern) and statistics of the scattering amplitude. Each term in (2) for the case in which there is only one clutter feature (that is, $N = 1$) is illustrated (Fig. 2). Because of the beampattern effects, the convolved signal is shown to have a tail elevated above the Rayleigh pdf.

Ehrenberg evaluated (2) ($N = 1$; no "i") for the case of a scatterer randomly located in the beam from a monostatic circular transducer. He showed that the echo pdf associated with a scatterer randomly located in the beam was strongly non-Rayleigh. Chu and Stanton revisited Ehrenberg's approach by accounting for an arbitrary number of scatterers N, each randomly located in the beam, as formulated in (1a) [6]. The echo pdf $p_E^\Sigma(\tilde{e})$ was calculated through two approaches: a numerical evaluation of the statistics of (1a) and an analytical representation of the statistics of (1a) making use of compact formulas derived by Barakat [18]. The two approaches are mathematically equivalent, which was confirmed by the excellent comparison between the results from both approaches [6]. The Barakat approach provides compact analytical formulas for calculating the signal magnitude due to the addition of N independent complex random variables. Although the variables were arbitrary, beampattern effects are not explicitly accounted for. The approach involved use of characteristic functions. A key aspect of his derivation is applying the 1-D results from the method of characteristic functions to the 2-D case (i.e., a complex signal). Chu and Stanton used the Barakat formulas by first describing the statistics of $\tilde{e}_i$ in (1a) through the use of (2). The statistics of $\tilde{e}$ in (1a) were then calculated using Barakat's approach. Thus, effects due to the beampattern and statistics of scattering from individual scatterers (before beampattern effects) appeared explicitly in the characteristic-function-based formulation.

Although the characteristic-function-based approach involves a more compact set of equations, there are convergence issues associated with summing zeroes of the zeroth-order Bessel function [6]. Although, in each case, we have reached convergence, the numerical approach, initially used only for validation, has proven to be easier overall to calculate (i.e., less computer time). Thus, in this paper, we will show only the numerical results involving direct evaluation of the statistics of (1a) for the cases involving $N > 1$. The characteristic-function-based approach for $N > 1$ (i.e., via use of the Barakat formulations from [6]) provided the same results (not shown) as the numerical computations. The case of $N = 1$ involves direct use of (2).

In the cases involving the use of (2) for $N = 1$ and the use of characteristic functions (not shown) for $N > 1$, the beampattern pdf as illustrated in Fig. 2 was numerically calculated using

Ehrenberg's (B1), which is a general formula for asymmetrical beams [10]. We applied this formula to the case of the rectangular aperture analyzed in this paper and adapted it to amplitude statistics as described above.

Details of the numerical evaluation of the statistics of $\tilde{e}$ in (1a) for $N > 1$ are given in [16]. To summarize, realizations of $|f_i|$ are simulated by drawing independent samples from Rayleigh-distributed signals. The mean of each Rayleigh is assumed to be the same in this particular study, although, in general, the distribution used for each scatterer and its mean can be arbitrary and different from each other. These magnitudes are further modulated by values of the beampattern randomized through randomizing the location of the scatterer in the beam. The beampattern is calculated with the same rectangular aperture as used to collect the data as described above. Although Lee and Stanton [16] used the beampattern for a circular transducer (versus a rectangular aperture in this paper), the random sampling approach was identical. Specifically, in the software, the b variable for the circular transducer was simply replaced by the b variable for the rectangular transducer. Functionally, the pdfs associated with the two beampatterns are qualitatively similar in that they both generally decrease monotonically with amplitude, they both have constant slopes for high values of amplitude, and they both have fine structure associated with sidelobes. Many statistically independent realizations of (1a) are calculated in order to calculate $p_E^\Sigma(\tilde{e})$. The arguments of the pdfs are first normalized by their root mean square (rms) values (rms over the statistical ensemble) before the pdfs are normalized by their area.

Predictions of the echo statistics associated with a range of numbers of unresolved clutter features in the beam are illustrated (Fig. 3). Equation (2) is used directly for the case of $N = 1$ and (1a) is numerically evaluated, as described above, for $N > 1$. For each case, the echo pdf from each clutter feature (before beampattern effects) is a Rayleigh pdf, each with the same mean. As with Fig. 2, the Rayleigh pdf due to one clutter feature (before beampattern effects) is illustrated with a thick solid curve. Also shown is the probability of false alarm (PFA), which is calculated from the expression (1-cdf), where cdf is the cumulative density function, based on the pdf. Both the pdf and PFA are shown to have a higher tail than for the Rayleigh case for each value of N. The predictions indicate that the fewer the number of unresolved clutter features in the sonar resolution cell, the higher the tail.

Last, a two-component mixed pdf is used in the analysis of the clutter data to account for a diffuse Rayleigh background and to better fit the full range of echo values

$$p_{\text{mix}}(\tilde{e}) = w p_E^\Sigma(\tilde{e}) + (1 - w) p_R(\tilde{e}) \qquad (3)$$

where p_R is the Rayleigh pdf, $p_E^\Sigma(\tilde{e})$ is the pdf of ($\tilde{e}$) as calculated from (1a) ($N > 1$) or (2) ($N = 1$, no "Σ" superscript notation), and the clutter fraction w is a constant in the range $0 \le w \le 1$.

III. COMPARISONS OF PREDICTIONS WITH CLUTTER DATA

The clutter data from the horizontal-looking sonar in [5] were collected in sample windows of the same size and at approx-
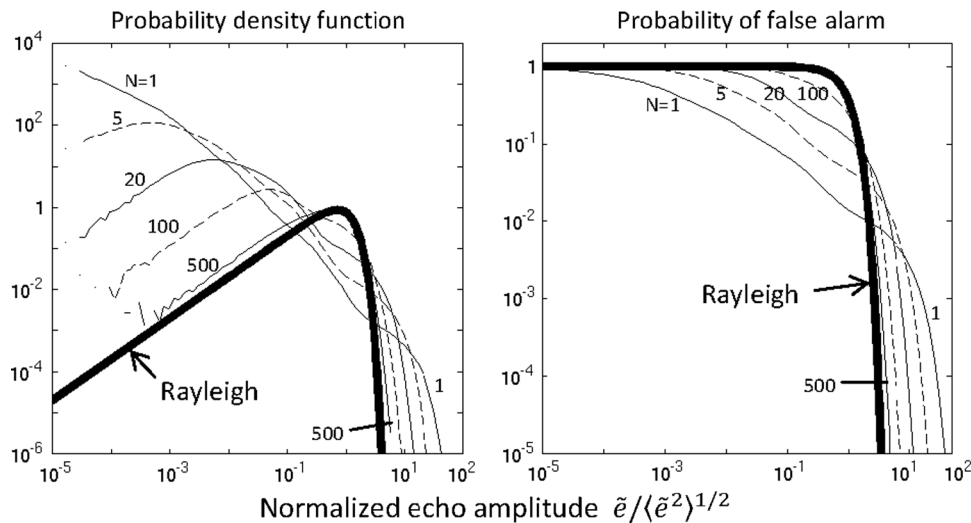
Fig. 3. Echo statistics for N unresolved scatterers randomly distributed in a sonar beam for the cases of $N = 1, 5, 20, 100,$ and 500. The echo from each scatterer is Rayleigh distributed (before beampattern effects) with the same mean. Although not all of the curves are labeled for each value of N, they appear in sequence. The values of N correspond to the total number of scatterers in a half-space (i.e., including mainlobe and all sidelobes).

imately the same range (distance from sonar) so that comparisons of the echo statistics could be made between windows. For example, sample windows of different sizes and/or at different ranges for the same type of clutter could result in a different number of clutter features insonified. In such a case, the shape parameter [e.g., N in (1a)] of the statistics could vary from window to window which would prevent rigorous comparisons. Furthermore, all chosen clutter data involve the direct-path case in which there are no interfering echoes from neighboring boundaries. This allows direct comparison with the direct path predictions described above.

Approximately 10 000 data points were used to form each data histogram. The data from each ping are first "normalized" using a split-window normalizer (SWN) as described in [5]. In particular, the sample of interest is divided by noise averaged in local cells, i.e., a cell-averaging constant false alarm rate (CA–CFAR) method [19]. The normalized signal is, in essence, the signal-to-background ratio. The normalized data were not thresholded for this current analysis. The data were further normalized by its rms level across all points in a sample window as shown in the figure labels. The inverse bandwidth (5 ms) of the signal was much smaller than the gap in the first normalization window and, hence, the statistics were driven by the inverse bandwidth (related to resolution cell), not the window.

Environmental data are not available for these sonar data, thus assumptions on the scattering characteristics of the clutter features must be made, which limits the analysis to qualitative comparisons. A major assumption in the modeling is that each clutter feature has a Rayleigh-distributed echo (before beampattern effects) with the same mean value. As described above, the model is general enough to account for other distributions and of unequal means.

PFAs calculated from the data are compared with predictions of PFAs based on calculations of pdfs using (2) for $N = 1$ and (1a) for $N > 1$ as described above (Fig. 4). A PFA based on a Rayleigh pdf (no beampattern effects) is shown for comparison. All data are shown to be strongly non-Rayleigh with tails elevated above the Rayleigh-based PFA that does not include

beampattern effects. Also, there is general qualitative agreement between the tails of most of the data and the predictions that include beampattern effects. There are significant departures between most data and predictions for smaller values of echo amplitude, where the theory greatly underpredicts the data. There are also departures between some of the data and predictions at the higher values of echo amplitude. As discussed in [5], there is also a trend of the tails of the CNS data being higher than those of the CS which, in turn, are higher than the BL tails.

To address the discrepancies between predictions and data for lower echo amplitudes, PFAs were also calculated using a mixed two-component pdf from (3) (Fig. 5). Here, one component is a Rayleigh pdf (without beampattern effects) and the other component is from (2) for $N = 1$ and from (1a) for $N > 1$. Using a least squares approach and through varying the mixed pdf clutter fraction w and N, the comparison between the resultant best fit predictions (thin solid curve) with the data (thick dashed curve) is superior compared with the best fit one-component PFAs (thin dashed curve) over the entire range of echo amplitudes. A PFA based on a Rayleigh pdf (no beampattern effects; thick solid curve) is shown for comparison. There still remain some discrepancies between predictions and data for lower values of echo amplitude, although the discrepancies were significantly reduced over the case of the one-component PFA. Also, there remain some discrepancies at the highest values of the tails, such as the middle CNS plot [Fig. 5(h)].

The variables N [from (1a)] and w [from (3)] were varied independently from 1 to 1000 and from 0 to 1, respectively, in the calculations of many classes of curves of the PFA [one curve from (3) per (N, w) pair] in this least squares process. The (N, w) pair associated with the least squares difference between the predicted PFA curve and the data represents the inferred number and clutter fraction of the scatterers, as shown in Table I.

Several least squares approaches were attempted to obtain a best fit (not shown). Note that in [7] and [8], an expectation–maximization algorithm was used to provide a maximum-likelihood parameter estimate in their fit of the theoretical pdfs to the data. The approach we chose for Fig. 5 involved calcu-
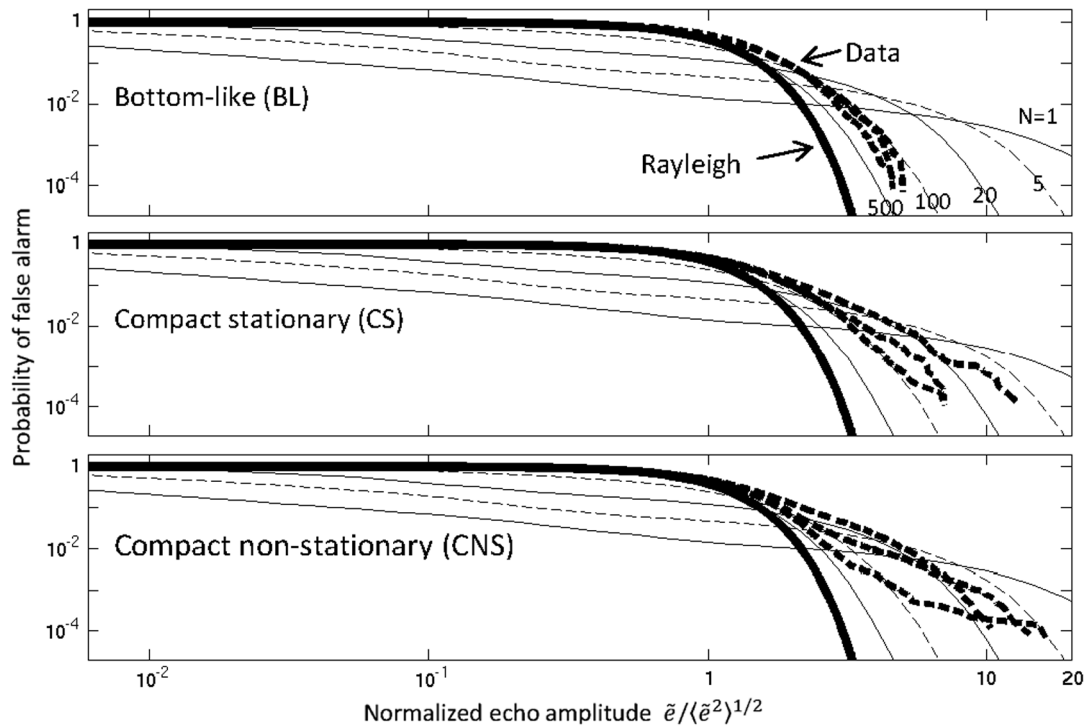
Fig. 4. Comparisons between theoretical PFAs from the right panel of Fig. 3 (thick solid curve and thin solid and dashed curves) and the three classes of clutter data (thick dashed curves). Each class has three independent sets of data.
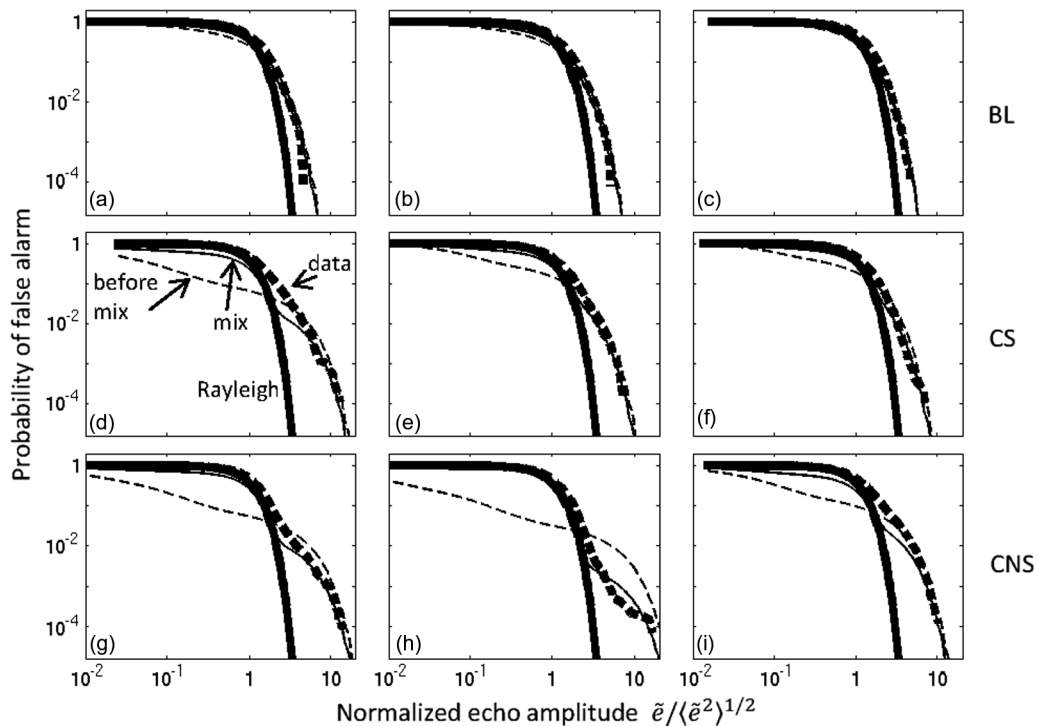

Fig. 5. Comparisons between best fit of PFA based on mixed pdf from (3) (thin solid curve) and each set of data (thick dashed curve). The one-component beampattern-based PFA based solely on p_E^Σ (thin dashed curve) that was best fit to the data and PFA based on a Rayleigh pdf (thick solid curve) are shown for comparison. Values of N and w inferred from the best fits are given in Table I. As in Figs. 3 and 4, the values of N correspond to the total number of scatterers in a half-space. These values are scaled in the analysis to the number of scatterers in the mainlobe of the beam and are also listed in Table I.

lating the differences of the PFAs on a log scale. In addition, the echo amplitudes were equally spaced on a log scale. Through this process, both the low and high echo amplitudes, as well as low and high PFA values, were given equal weight. Because of the high computational times to calculate the pdfs in this current work, a finite number of values of N were used in the inferences,

as listed in the caption to Table I. This results in discrete integer values of N, with small spacing (unity) for small values of N and large spacing (100) for large values of N.

The model-estimated values of the number of scatterers (N) involve the entire half-space. This is a natural outcome of modeling the echoes from a sonar system since the beam "sees"

TABLE I
MODEL PARAMETERS USED IN PREDICTING PFAS BASED ON (3) IN FIG. 5(A)–(I). THE TERM N IS BASED ON PREDICTIONS USING (2) [IN (3)] FOR $N = 1$ AND (1A) [IN (3)] FOR $N > 1$ AND REPRESENTS THE TOTAL NUMBER OF SCATTERERS IN A HALF-SPACE WITHIN THE SONAR RANGE RESOLUTION CELL (I.E., INCLUDING MAINLOBE AND ALL SIDELOBES). IN THE ADJACENT COLUMN, THE VALUES OF N ARE SCALED FOR THE AVERAGE NUMBER OF SCATTERERS IN A RANGE RESOLUTION CELL WITHIN THE MAINLOBE OF THE BEAM (I.E., WITHIN THE FIRST NULL). THE TERM w IS ASSOCIATED WITH THE TWO-COMPONENT MIXED PDF FROM (3) AND REPRESENTS THE FRACTION OF THE PDF THAT IS DUE TO CLUTTER [I.E., $p_E^\Sigma(\tilde{e})$ FROM (3)], 37 VALUES OF N WERE USED IN THE INFERENCES: 1, 2, 3,...... 20, 30, 40,......... 100, 200, 300, ... 1000

Clutter type	panel	N (half-space)	Average number within mainlobe	w (clutter fraction)
Bottom-like (BL)	a	100	2.5	0.60
	b	100	2.5	0.65
	c	200	5.1	0.80
Compact stationary (CS)	d	8	0.20	0.45
	e	30	0.76	0.45
	f	50	1.3	0.45
Compact non-stationary (CNS)	g	6	0.15	0.35
	h	3	0.076	0.15
	i	14	0.36	0.50

in all directions. For this case of a narrow beam ($5° \times 20°$), most of the inferred scatterers are in the sidelobes of the beam-pattern and only a relatively few will be, on average, in the mainlobe. In many systems, only the echoes above a certain threshold are analyzed, which corresponds to the "tail" of the echo pdf. The tail will generally correspond to dominant echoes such as those due to scatterers in the mainlobe of the sonar beam. Thus, it is convenient to use these model results to estimate those numbers. Through simple geometrical arguments, the inferred number of scatterers subtended solely by the mainlobe is calculated by scaling N by the ratio of the solid angle subtended by the mainlobe (0.1595 rad) and the half-space solid angle (2π rad) (Table I). For simplicity, the mainlobe is considered to be the portion of the beam within the first null of the mainlobe. This line of delineation is chosen over, for example, the -3-dB points, because the echo statistics are strongly influenced by most of the mainlobe down to near the nulls. However, in general, the estimates of the dominant scatterers will involve system-specific noise. The average number of scatterers within the mainlobe is estimated to be in the ranges 2.5–5.1 (BL), 0.20–1.3 (CS), and 0.076–0.36 (CNS) (Table I). This trend indicates that the inferred number of scatterers within the mainlobe changes with changing clutter type from highest values with BL, to intermediate values with CS, and to lowest values with CNS. The tails are correspondingly "heavier" in the progression of BL to CS to CNS (Fig. 5).

IV. DISCUSSION AND CONCLUSION

Through the use of a recently developed model of echo statistics, there was generally good qualitative agreement between predictions using this model and the tails of three classes of clutter data as measured at midfrequencies. The model rigorously accounts for the average number of scattering features within a sonar resolution cell, the statistical properties of their echoes (before beampattern effects), and beampattern effects. Through implementing this model in a two-component mixed pdf, with the other pdf being Rayleigh, the entire range of values of echo amplitude was reasonably predicted. This general agreement between the shape of the predicted pdf curves and the

shape of the experimental pdf curves was the first experimental validation of this exact model. Furthermore, this comparison provided inferences of number of scatterers per sonar resolution cell for each type of clutter.

As discussed above, the vast majority of echoes from clutter features within a sample window are from the sidelobes. Although the tail of the clutter predictions provides reasonable fits to most clutter echoes with high values, the pure Rayleigh component of the mixed pdf was required to predict the PFA for lower values of echo amplitude. The need for this component can be explained by the presence of either the background system noise, diffuse reverberation, or some combination that dominated the signal for low values. Diffuse reverberation, in this context, would involve scattering by a randomly distributed array of scattering features, with many of the features contributing to each echo. With a large enough number of these features, the resultant statistics, through the central limit theorem, would be Rayleigh distributed even with beampattern effects included.

The analysis was limited, in large part, by the absence of environmental data. Thus, the analysis focused on a qualitative study examining the trends of the data in relation to the predictions. Nonetheless, comparison between the predicted and observed trends served as experimental validation of the model. Furthermore, quantitative inferences could be made with assumptions. For example, the average number of scattering features in each sonar range resolution cell within the mainlobe was inferred. This inference demonstrated that, in general, the bottom-like clutter involved the largest number of scattering features, and the compact stationary and compact nonstationary clutter involved an intermediate and smallest number of features, respectively. This trend is consistent with the fact that the tails of the echoes are increasingly elevated in the progression of BL to CS to CNS clutter types.

The elevated portions of the tails not predicted by the theory are possibly due to deviations from the assumptions that the clutter features: 1) were Rayleigh distributed (before beampattern effects); 2) had the same mean value; and 3) were uniformly distributed (stationary statistics). For example, deviations from

predictions are particularly apparent in Fig. 5(h) where the tail of the data does not follow the slope of the predictions. This may be the cause of the large difference in inferred N and w for these data compared with the values of N and w, respectively, for the other CNS data. Not accounting for these deviations translates to the inferred number of scatterers and clutter fraction being effective values of number and clutter fraction, respectively, for this particular set of assumed scattering parameters. Also, as discussed above, the fact that the predictions required a two-component pdf, with one being a Rayleigh, suggests that more is contributing to the echo than finite numbers of large clutter features. When realizations of the clutter give rise to clutter echoes that are smaller than the background signal, the use of a simple two-component mixture pdf can also give rise to errors in inferred values of N and w as described below.

It has recently been demonstrated that the echoes from randomly oriented, randomly rough, elongated objects are non-Rayleigh before beampattern effects [14], [15]. For that type of scatterer, the inferred number of scatterers in this paper's data would be higher than in the assumed case of Rayleigh scatterers. The case of mixed assemblages of dissimilar scatterers whose mean echoes are different has also been recently examined [16]. The degree to which the echo from a mixed assemblage was non-Rayleigh was not only related to the number of scatterers, but also to the ratio of their individual scattering amplitudes. This demonstrates that the inferred number of scatterers will vary with the mixture, such as in the case of a mix of BL, CS, and/or CNS in the same sample window.

The work on mixed assemblages also demonstrates the conditions under which the inferred clutter fraction w in this paper is accurate [16]. If the distribution of scatterers is simply split into two separate regions of mono-type scatterers, then the clutter fraction is interpreted directly and accurately in terms of the proportion of area containing the clutter echoes. Also, if the dominant scatterer is sparsely distributed, then w is accurate. However, if there is a mixture of different scatterer types interspersed within a resolution cell, then the error in w can be significant. The values of w in Table I are shown to vary slightly with inferred number of scatterers in the resolution cell. If there is no error in inferred values of N and w, then these results would suggest that with these three different clutter types, as the fraction of area containing the clutter area increases, so does the numerical density of the clutter features within the area. However, there is probably error in the inferred values of w, especially for the BL cases where there are multiple clutter features per resolution cell and the possibility that those features are a mix of different scatterer types.

Finally, the predictions and data were associated with direct path echoes. There are also important cases in which interactions with neighboring boundaries (waveguide effects) of a long-range sonar will interfere with the direct path echoes and need to be accounted for. In this case, the pdfs will tend to be "whitened" (i.e., become more Rayleigh-like) as the number of interactions increases [20], although there are important conditions under which the echoes can still remain strongly non-Rayleigh after waveguide effects [17].

Despite the limitations in the analysis, the qualitative agreement between predictions and data showed the value of the new approach as well as served as a first experimental validation of the model. Future studies and more in-depth validation should include using sonar data that has environmental data of sufficient detail that the degree to which echoes from individual scattering features might be non-Rayleigh before beampattern effects, the statistics of the means of their echoes, as well as the stationarity of the clutter field can be quantified. Also, with the new methods developed in [17], predicting echo statistics associated with beampattern and various clutter types detected by a long-range sonar where waveguide effects are important is now possible.

REFERENCES

[1] E. Jakeman and P. N. Pusey, "A model for non-Rayleigh sea echo," *IEEE Trans. Antennas Propag.*, vol. AP-24, no. 6, pp. 806–814, Nov. 1976.

[2] D. A. Abraham and A. P. Lyons, "Novel physical interpretations of K-distribution reverberation," *IEEE J. Ocean. Eng.*, vol. 27, no. 4, pp. 800–813, Oct. 2002.

[3] T. K. Stanton and D. Chu, "Non-Rayleigh echoes from resolved individuals and patches of resonant fish at 2–4 kHz," *IEEE J. Ocean. Eng.*, vol. 35, no. 2, pp. 152–163, Apr. 2010.

[4] B. R. La Cour, "Statistical characterization of active sonar reverberation using extreme value theory," *IEEE J. Ocean. Eng.*, vol. 29, no. 2, pp. 310–319, Apr. 2004.

[5] J. M. Gelb, R. E. Heath, and G. L. Tipple, "Statistics of distinct clutter classes in midfrequency active sonar," *IEEE J. Ocean. Eng.*, vol. 35, no. 2, pp. 220–229, Apr. 2010.

[6] D. Chu and T. K. Stanton, "Statistics of echoes from a directional sonar beam insonifying finite numbers of single scatterers and patches of scatterers," *IEEE J. Ocean. Eng.*, vol. 35, no. 2, pp. 267–277, Apr. 2010.

[7] D. A. Abraham, J. M. Gelb, and A. W. Oldag, "K-Rayleigh mixture model for sparse active sonar clutter," in *Proc. OCEANS Conf.*, Sydney, Australia, May 2010, DOI: 10.1109/OCEANSSYD.2010.5603815.

[8] D. A. Abraham, J. M. Gelb, and A. W. Oldag, "Background and clutter mixture distributions for active sonar statistics," *IEEE J. Ocean. Eng.*, vol. 36, no. 2, pp. 231–247, Apr. 2011.

[9] J. W. Goodman, *Statistical Optics.* New York, NY, USA: Wiley, 1985, ch. 2.

[10] J. E. Ehrenberg, "A method for extracting the fish target strength distribution from acoustic echoes," in *Proc. Conf. Eng. Ocean Environ.*, 1972, vol. 1, pp. 61–64.

[11] J. E. Ehrenberg, T. J. Carlson, J. J. Traynor, and N. J. Williamson, "Indirect measurement of the mean acoustic backscattering cross section of fish," *J. Acoust. Soc. Amer.*, vol. 69, pp. 955–962, 1981.

[12] J. E. Ehrenberg, "A review of target strength estimation techniques," in *Underwater Acoustic Data Processing*, Y. T. Chan, Ed. Dordrecht, The Netherlands: Kluwer, 1989, pp. 161–175.

[13] T. K. Stanton and C. S. Clay, "Sonar echo statistics as a remote sensing tool: Volume and sea floor," *IEEE J. Ocean. Eng.*, vol. OE-11, no. 1, pp. 79–96, Jan. 1986.

[14] S. Bhatia, "Non-Rayleigh scattering by a randomly oriented elongated scatterer," S.M. thesis, Appl. Ocean Sci. Eng., Massachusetts Inst. Technol./Woods Hole Oceanogr. Inst., Cambridge/Woods Hole, MA, USA, Sep. 2012.

[15] S. Bhatia, T. K. Stanton, and K. Baik, "Non-Rayleigh scattering by a randomly oriented elongated scatterer randomly located in a beam," *IEEE J. Ocean. Eng.*, 2014, DOI: 10.1109/JOE.2013.2293959.

[16] W.-J. Lee and T. K. Stanton, "Statistics of echoes from mixed assemblages of scatterers with different scattering amplitudes and numerical densities," *IEEE J. Ocean. Eng.*, 2014, DOI: 10.1109/JOE.2013.2285657.

[17] B. A. Jones, J. A. Colosi, and T. K. Stanton, "Echo statistics of individual and aggregations of scatterers in the water column of a random, oceanic waveguide," *J. Acoust. Soc. Amer.*, vol. 136 [Online]. Available: http://dx.doi.org/10.1121/1.4881925

[18] R. Barakat, "First-order statistics of combined random sinusoidal waves with applications to laser speckle patterns," *Optica Acta*, vol. 21, pp. 903–921, 1974.

[19] B. R. Mahafza, *Radar Systems Analysis and Design Using MATLAB*. London, U.K.: Chapman & Hall/CRC Press, 2013, ch. 13.

[20] D. A. Abraham, "The effect of multipath on the envelope statistics of bottom clutter," *IEEE J. Ocean. Eng.*, vol. 32, no. 4, pp. 848–861, Oct. 2007.

Timothy K. Stanton received the B.S. degree from Oakland University, Rochester, MI, USA, in 1974 and the M.S. and Ph.D. degrees from Brown University, Providence, RI, USA, in 1977 and 1978, respectively, all in physics. His undergraduate research involved experiments in solid-state acoustics with Dr. N. Tepley as advisor and his graduate research involved nonlinear acoustics measurements and instrumentation development with Dr. R. Beyer as advisor.

From 1978 to 1980, he was a Senior Engineer with the Submarine Signal Division, Raytheon Company, Portsmouth, RI, USA, where he was engaged in research, development, and testing of acoustic systems. From 1980 to 1988, he was a Member of the Scientific Staff, Department of Geology and Geophysics, University of Wisconsin, Madison, WI, USA, where he conducted various theoretical, laboratory, and field studies in acoustical oceanography with Dr. C. Clay. From 1988 to the present, he has been a Member of the Scientific Staff, Department of Applied Ocean Physics and Engineering, Woods Hole Oceanographic Institution (WHOI), Woods Hole, MA, USA. From 1997 to 2001, he was Chair of the Department and currently is a Senior Scientist. He is collaborating with colleagues in the development of models of acoustic scattering by marine organisms through various theoretical and laboratory methods, physics-based models of the statistics of scattered signals, and is applying the models to ocean measurements. In addition to his research, he is part of the Massachusetts Institute of Technology (MIT), Cambridge, MA, USA and WHOI Joint Graduate Education Program and teaches acoustic scattering theory. Overall he has published papers covering the areas of nonlinear acoustics, acoustics instrumentation, fiber-optic hydrophones, echo statistics, and acoustic scattering by volumetric objects, seafloor, sea surface, and the underside of sea ice.

Dr. Stanton has served as an Associate Editor for the *Journal of the Acoustical Society of America* and as a Guest Editor for a special issue of Deep Sea Research. He has also served as a Guest Editor for a special issue of the IEEE JOURNAL OF OCEANIC ENGINEERING. He is a Fellow of the Acoustical Society of America and is a Member of The Oceanography Society. In 1985, he was awarded the A.B. Wood medal for Distinguished Contributions to Underwater Acoustics. He has held the Adams Chair at WHOI since 2011.

Dezhang Chu received the B.A. degree in electrical engineering from the China University of Geosciences, Wuhan, China, in 1982 and the Ph.D. degree in geophysics from the University of Wisconsin, Madison, WI, USA, in 1989.

He was a Postdoctoral Scholar from 1989 to 1990 and a Postdoctoral Investigator from 1990 to 1991 with the Woods Hole Oceanographic Institution (WHOI), Woods Hole, MA, USA. From 1991 to 2007, he was first a Research Associate and then a Research Specialist with the Department of Applied Ocean Physics and Engineering, WHOI. During that period at WHOI, he developed acoustic scattering models for zooplankton, fish, and seafloor, conducted laboratory and ocean measurements of scattering, as well as developed signal processing methods for acoustic scattering by marine organisms. Since 2007, he has been with the Acoustics Team of the NOAA/NMFS Northwest Fisheries Science Center (NWFSC), Fishery Resources Analysis and Monitoring Division, Seattle, WA, USA. Currently, his research is focused on acoustic scattering, characterization, and classification of fish.

Dr. Chu is a Fellow of the Acoustical Society of America.

James M. Gelb (M'02) was born in Los Angeles, CA, USA, in 1963. He received the B.A. degree in mathematics from the University of California at Los Angeles (UCLA), Los Angeles, CA, USA, in 1985 and the Ph.D. degree in theoretical physics from the Massachusetts Institute of Technology (MIT), Cambridge, MA, USA, in 1992.

Currently, he is a Research Scientist at the Signal and Information Sciences Laboratory, Signal Physics Division, Applied Research Laboratories, University of Texas at Austin (ARL:UT), Austin, TX, USA, specializing in midfrequency active sonar. His technical experience includes general analytic and numerical modeling and algorithm development across disciplines (e.g., physics, engineering, and finance) with over 40 journal publications including highly referenced publications on solar neutrino physics and cosmological simulations. His sonar experience includes signal processing techniques and tracking and classification research with a current focus on clutter modeling and statistics. He is currently developing a program in musical acoustics. His past positions include: research staff at the Fermi National Accelerator Laboratory (Fermilab), Batavia, IL, USA and the Los Alamos National Laboratory, Los Alamos, NM, USA; a Derivatives Quantitative Researcher at Morgan Stanley; and the Director of Astronomy at the University of Texas at Arlington, Arlington, TX, USA

George L. Tipple (S'08) was born in Bridgeport, CT, USA, in 1986. He received the B.S. degree in electrical engineering with special interests in computer hardware and circuit design from the University of Texas at Austin, Austin, TX, USA, in 2009.

He has four years of experience as a student technician in midfrequency active sonar at the Applied Research Laboratories, University of Texas at Austin (ARL:UT), including computational support for clutter modeling and tracking and classification algorithms. He is currently working in the computer industry.

Kyungmin Baik received the B.S. and M.S. degrees in physics from Korea University, Seoul, Korea, in 1996 and 2000, respectively, and the Ph.D. degree in physics from Washington State University, Pullman, WA, USA, in 2008, under the supervision of Dr. P. L. Marston.

He was a Research Fellow at the Institution of Sound and Vibration Research, University of Southampton, Southampton, U.K., from 2008 to 2010, under the supervision of Dr. T. G. Leighton and was a Postdoctoral Scholar at the Woods Hole Oceanographic Institution (WHOI), Woods Hole, MA, USA, from 2010 to 2012, under the supervision of Dr. T. K. Stanton. He has been a Senior Researcher at the Korea Research Institute of Standards and Science, Daejeon, Korea, since 2012. Overall, his research has focused on acoustic scattering by various types of objects, including bubbles, elongated objects, and objects on an interface.

Dr. Baik is a member of the Acoustical Society of America.